



HAL
open science

Non-linear Ultrasonic Computed Tomography (USCT) for soft and hard tissue imaging

P. Lasaygues, J. Rouyer, S. Mensah, E Franceschini, G Rabau, R Guillermin,
Samuel Bernard, V. Monteiller, Dimitri Komatitsch

► **To cite this version:**

P. Lasaygues, J. Rouyer, S. Mensah, E Franceschini, G Rabau, et al.. Non-linear Ultrasonic Computed Tomography (USCT) for soft and hard tissue imaging. International Workshop on Medical Ultrasound Tomography, Nov 2017, Speyer, Germany. hal-01769814

HAL Id: hal-01769814

<https://hal.science/hal-01769814>

Submitted on 18 Apr 2018

HAL is a multi-disciplinary open access archive for the deposit and dissemination of scientific research documents, whether they are published or not. The documents may come from teaching and research institutions in France or abroad, or from public or private research centers.

L'archive ouverte pluridisciplinaire **HAL**, est destinée au dépôt et à la diffusion de documents scientifiques de niveau recherche, publiés ou non, émanant des établissements d'enseignement et de recherche français ou étrangers, des laboratoires publics ou privés.

Non-linear Ultrasonic Computed Tomography (USCT) for soft and hard tissue imaging

P. Lasaygues, J. Rouyer, S. Mensah, E. Franceschini, G. Rabau, R. Guillermin, S. Bernard, V. Monteiller, D. Komatitsch

Aix Marseille Univ, CNRS, Centrale Marseille, LMA, Marseille, France

E-mail: lasaygues@lma.cnrs-mrs.fr

Abstract

Ultrasonic Computed Tomography (USCT) is an imaging technique that has proven effective for soft-tissue characterization. The classical tomography procedures are adapted to broadband data acquired in scattering configurations under Born approximation for homogeneous media and far-field conditions, while the heterogeneous objects are probed by spherical waves in near-field conditions. An elliptical Fourier transform theory is then derived to solve the near-field inverse problem in case of harmonic ellipsoidal waves. More recently, the use of USCT has been envisaged for bone imaging. In this field, the large variations of impedance distribution (high impedance contrast) require that the modelling of wave propagation be integrated into the reconstruction scheme. In that case, iterative inversion schemes are proposed. These various reconstruction procedures are validated against experiments and numerical simulations.

Keywords: Ultrasonic Computed Tomography, Inverse Born Approximation, Iterative Approximation, Full Waveform Imaging, Breast, Bones

1 Introduction

This paper presents the theoretical framework that enables to find specific responses, on the one hand, to the problem of soft tissue imaging (typically breast cancer detection) and, on the other hand, to the problem of bone characterization (typically osteoporosis, bone infection and cancer detection). The difficulties raised are somewhat different as in soft tissues the very small fluctuations to be quantified suffer from their very low values. This poor echogenic index generally induces low detection probability, for instance in the case of large diffuse masses. In addition, invasive lesions that must not be overlooked, may be of millimetric size. In bone imaging, the difficulties arise from the very high echogenic index of the bone that strongly alters the propagation of the ultrasonic waves. Solutions consist in optimally assessing these

non-linear effects in an iterative approach aiming at local linearization. In this paper, we describe a Ultrasonic Computed Tomography (USCT) method based on the use of the first-order inverse Born approximation (IBA) method, applied to the case of a homogeneous and constant background. The unknown object function, which is assumed to be weakly heterogeneous, is linearly related to the field measured via a spatial Fourier transform. The inverse problem is based on the filtered back-projection algorithm. However, such approaches are limited for breast inspection, in which the probe is either in contact with the skin or located within a near-field distance when using a coupling device (water bag or water tank). In this case, an extension of the method is proposed via a tool called Elliptical Fourier transform [1]–[3]. Nevertheless, the first-order Born USCT has some limitations when dealing with highly-contrasted scatterers. When the problem can be reduced to the study of a fluid-like cavity buried in an elastic cylinder surrounded by water, an extension of the IBA method can be proposed, taking into account physical phenomena such as wave refraction [4]. The first approach is purely experimental and consists in performing reflection and transmission measurements, using an iterative correction procedure, which compensates for refraction effects arising at the boundary between bone and the surrounding tissues. The main limitation of the method is the heavy experimental costs involved (multiple iterative experiments). We have then suggested a numerical non-linear inversion algorithm, in which the minimization procedure between the full recorded and simulated data is performed using a Polak-Ribière conjugate-gradient method mainly developed in non-destructive testing domain, or an efficient quasi-Newton technique mainly developed in seismology (related to the full waveform inversion method). An overview of the performances and the limitations of these tomography methods applied to breast and bone imaging problems are presented and discussed.

2 USCT Formulation

2.1 Physical background

Ultrasonic Computed Tomography (USCT) applied to soft tissues has been studied in several publications [5]–[8], and the use of powerful computers makes it possible nowadays to introduce more complex algorithms [1], [9]. Numerous experimental devices have been developed [10]–[12].

Let A be the operator that describes the acoustic propagation or the scattering phenomena in the heterogeneous medium of interest (including boundary and/or Sommerfeld conditions). Let S be the acoustic sources, which are assumed to be known. The variable φ denotes the resulting acoustic field, and satisfies the equation:

$$\text{Eq. 1: } A\varphi = S$$

Let us assume the medium to be composed of a known domain (the reference medium as the background) resulting in an operator A_0 , and an unknown domain (the object) resulting in an operator A' such as:

$$\text{Eq. 2: } A = A_0 + A'$$

Assuming that φ_0 , the solution of the unperturbed problem, is known:

$$\text{Eq. 3: } A_0 \varphi_0 = S$$

Let φ' be the difference between φ and φ_0 , that is the field perturbation induced by the perturbation by the object of the reference medium. Therefore φ' is the solution of

$$\text{Eq. 4: } A_0 \varphi' = -A'(\varphi_0 + \varphi')$$

If the Green function G_0 of the unperturbed problem is given by $G_0 = -A_0^{-1}$, the Eq. 4 can be written:

$$\text{Eq. 5: } \varphi' = G_0 A'(\varphi_0 + \varphi')$$

The latter equation is the Lippmann-Schwinger non-linear equation, and a solution can be found by using a perturbation scheme, based on successive linear approximations. The "Born series" is one of these schemes introducing different development orders. Within the first-order Born approximation, the field perturbation φ' is neglected in every internal point of the scatterer. The solution φ'_1 can be written:

$$\text{Eq. 6: } \varphi'_1 = G_0 A' \varphi_0$$

In the frequency range (> 3 MHz) of USCT of weakly heterogeneous soft tissues, in first approximation the reference medium is considered to be constant, leading to an Inverse Born Approximation (IBA) method with a constant background. The final objective is to obtain suitable images from scattered measurements $(\varphi')^m$, where the subscript m stands for measurements. Rotating the transducers around the object and transmitting broadband pulses at each angular position can be handled using the same approach as in X-ray tomography. This provides a slice-by-slice spectral coverage of the object spectrum ($2D$ -spatial Fourier transform, F_{2D}):

$$\text{Eq. 7: } A' = (F_{2D}^{-1}) (\varphi')^m$$

where (F_{2D}^{-1}) denotes the inverse two-dimensional spatial Fourier transform. The first reconstruction method was then performed using a classical algorithm of the summation of filtered back-projections [1], [13], [14]. This IBA formulation assumes a far-field propagation hypothesis, but often the object to be inspected is excited in a near-field region by a spherical wave

(harmonic ellipsoidal waves). The functions of domain decomposition then have as spatial support an ellipse whose foci are the position of the transducers. This decomposition has been called the Elliptic Fourier Transform [2].

The expression of the diffracted field φ' depends on the transfer function of the medium, the wave number k , and the diffraction angle. Depending on the fluid or elastic configuration, the transfer function, denoted $H(\theta, \omega)$, can be written:

- for fluid modeling

$$\text{Eq. 8: } H(\theta, \omega) = k_0^2 [\hat{\gamma}_\chi + \hat{\gamma}_\rho \cos\theta] (\vec{K}) = -k_0^2 [\hat{\gamma}_z (1 - \cos\theta) + \hat{\gamma}_c (1 + \cos\theta)] (\vec{K}) ;$$

$$\text{Eq. 9: } \gamma_\chi = \frac{\chi - \chi_0}{\chi_0} ; \gamma_\rho = \frac{\rho - \rho_0}{\rho} ; \gamma_z = \log\left(\frac{Z}{Z_0}\right) ; \gamma_c = \frac{c^2 - c_0^2}{c^2} ;$$

- for elastic modeling

$$\text{Eq. 10: } H(\theta, \omega) = -k_0^2 [\hat{\gamma}_\lambda - \hat{\gamma}_\mu \cos\theta + 2\hat{\gamma}_\rho \cos\theta] (\vec{K}) ;$$

$$\text{Eq. 11: } \gamma_\lambda = \frac{\lambda}{\lambda_0 + 2\mu_0} , \gamma_\mu = \frac{\mu}{\lambda_0 + 2\mu_0} ;$$

$$\text{Eq. 12: } \vec{K} = k(\vec{n}_0 - \vec{n}) ; \cos\theta = \vec{n}_0 \cdot \vec{n} ;$$

with χ is the compressibility, ρ is the density, Z is the impedance, c is the compressional speed of sound, and λ, μ , are the Lamé coefficients. $\hat{\gamma}$ stands for the 2D elliptical Fourier transform of the parameter γ . The subscript "0" represents the parameters related to the background medium. \vec{n}_0 and \vec{n} are the normal vectors in the incidence direction and in the observed direction (θ is the diffraction angle). These equations involve the acoustic parameters offering distinct directivity patterns that can be separated according to spatial scanning performed: transmission ($\theta = 0^\circ$), reflection ($\theta = 180^\circ$) and diffraction ($\forall\theta$).

2.2 From soft to hard tissue modeling

With hard biological tissues, such as bones, having larger acoustic impedances than those of the surrounding medium, the weak scattering assumption is no longer realistic. Indeed, the path of the transmitted wave changes from its initial course because of refraction. This results in the propagation of more complex waves, such as those occurring in elastic volumes (compressional and shear waves). The weak scattering hypothesis is therefore not realistic.

Provided some assumptions, the application of USCT can be extended to bone imaging. If the object to be imaged can be modeled by a set of concentric isotropic homogeneous noncircular fluid-like media representing the homogenized surrounding tissues, bone and marrow, only

compressional waves are taken into account. Using low frequency transducers (< 3 MHz), the wavelength of the compressional wave (propagating at velocities ranging between 2000 and 4000 m.s⁻¹) in the cortical bone is typically greater than 1 mm, which remains much larger than the typical size of bone microstructures. Therefore, the cortical shell of the bone can be intrinsically seen as a weakly heterogeneous medium, and ultrasonic wave propagation will be minimally disturbed. Thus, the Born approximation is satisfied in this area. The IBA method with a variable background can be used; the background being the set consisting of the homogeneous solid cylinder and the homogeneous fluid surrounding medium. The solution φ'_1 can be then written:

$$\text{Eq. 13: } \varphi'_1 = G_p A' \varphi_b$$

where G_p is the suitable Green function of the variable background. φ_b and A_b are respectively the corresponding field and the corresponding operator such as:

$$\text{Eq. 14: } A_b \varphi_b = S \text{ and } A_b G_b = I$$

where I is the identity operator. The strategy can be applied iteratively:

$$\text{Eq. 15: } \varphi'_n = G_b^{n-1} A'_n \varphi_b^{n-1}$$

where G_b^n is the inhomogeneous Green function of the variable background adapted for every iteration step n . This non-linear inversion scheme is called Compound USCT, and the reconstruction algorithm is therefore the same as the previous classical one. The solutions are iteratively determined using Eq. 7. Experimentally, this approach was adapted to bone sample considered as a tube-like sample. The refraction effects are cancelled using a specific set-up in order to impose straight ray propagation inside the shell of the tube/bone [4]. Despite limitations due to heavy data processing requirements and complex acoustic signals resulting from multiple physical effects involved (various paths into the shell, roughness of the water/bone interfaces etc...), this approach gives images that are quantitatively related to the compressional wave velocities in a cross-section of a cortical shell, and the error remains within reasonable limits (about 7%).

A second non-linear inversion method was investigated. In this case, the medium is modeled without any *a priori* knowledge by performing a simple geometrical discretization of the object. The algorithm involves successive linearizations of the Lippmann-Schwinger representation. The initial guess in the iterative process is provided by the first-order Born approximation. If the solution is known with the order $(n-1)$, the n -order solution A'_n will satisfy:

$$\text{Eq. 16: } [(\varphi')^m - \varphi'_{n-1}] = G_b^{n-1} [A'_n - A'_{n-1}] \varphi_b^{n-1}$$

At each iteration, the algorithm numerically solves a forward diffraction problem in order to calculate the appropriate inhomogeneous Green function G_b^{n-1} and the internal field φ_b^{n-1} . Contrary to what occurs with the Compound USCT, this method requires only one series of experimental data, and involves the inversion of a huge, full and complex matrix. The matrix inversion procedure is the key point in this method. A mean-square solution can be calculated using a conjugate-gradient method associated with a regularization procedure. Our first approach is iterative, and the inversion procedure is carried out frequency by frequency from the sinogram in the frequency domain. The stability of the algorithm is improved using a Tikhonov regularization process. The minimization of the cost function (the difference between recorded and simulated waveforms) is computed using the Polak-Ribière conjugate gradient process. The detail of the algorithm is presented in [15], [16] for a numerical and experimental academic targets, and in [17] for a real lamb shoulder bone. To make use of the broadband frequency content of the impulse signal used, the idea is to begin with the low frequencies, which carry overall information, and to gradually inject the high frequencies to simultaneously improve both the qualitative aspects (the resolution) and the quantitative aspects (the characterization). However, this technique is computationally time consuming. The second proposed method consists in resorting to the more advanced Full Waveform Inversion (FWI) techniques that are at the forefront in the field of geophysics [18], [19]. The term "full" refers to the use of the full-time series. The aim is to simultaneously reconstruct the compression and shear waves in the bone without considering that the tissue density is spatially constant as in the previous method. Indeed, full waveform inversion is an imaging method that is based on full numerical modeling of wave propagation in the medium. The gradient of the cost function is obtained as the convolution product of the forward field with an adjoint field obtained by calculating the propagation of the time-reversed residuals. In this iterative process, some artifacts can alter the quality of the reconstruction. In order to reduce these artifacts and ensure a coherent reconstruction of the parameters, different pre-conditioning or regularization techniques can be proposed. The minimization of the cost function that we use is based on the quasi-Newton technique called Limited-memory Broyden-Fletcher-Goldfarb-Shanno (L-BFGS) [20], which is far more efficient in terms of convergence than conjugate-gradient techniques. The details of the algorithm are presented in [21].

3 Results

The feasibility of these different algorithms was tested on data obtained using mechanical and electrical ultrasonic scanners, allowing diffraction-, reflection- and/or transmission-mode measurements.

3.1 Breast phantom imaging

The breast training phantom CIRSTM Model 052A mimics the ultrasonic and anatomic characteristics of tissues found in an average patient. The soft tissue mimicking phantom made of

ZerdineTM contains cystic and solid masses which appear respectively dark and bright on B-mode (ultrasound sonography) and USCT images. B-mode images were made using a clinical ultrasound device, EsaoteTM AU5, with a 7-MHz linear probe. Near-field USCT images were made using the 1024-element electrical and mechanical scanner developed by our laboratory and presented in detail in [22]. Figure 1 shows, in the center, the USCT map of the analyzed phantom containing 5 dark masses and one bright mass. The two images on the side represent the B-mode images made of the areas of the phantom identified by the white rectangles. Differences arise because the scanner performs an entire 2D circular scan ($\varnothing = 30$ cm, 720 reflection measurements) around the breast phantom whereas a unique position of the probe (one incident direction) is considered with the B-mode system.

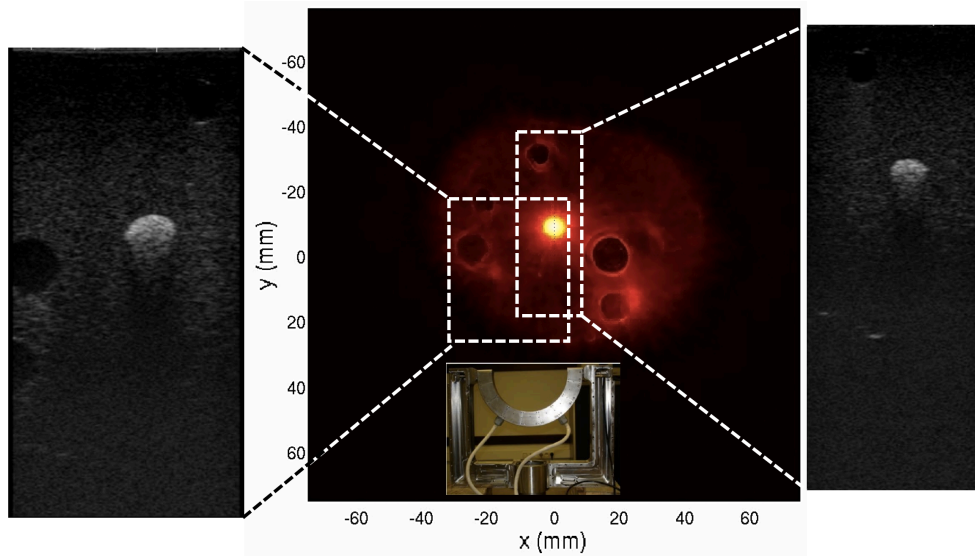


Figure 1: Imaging of the CIRSTM breast phantom. At the center, the USCT image (using the 1024-element scanner built by our laboratory), and on the sides, two B-mode images (using 7-MHz EsaoteTM AU5 scanner) of the areas marked by the white rectangles. The inlaid picture shows the semi-circular 1024-element array used. Details can be found in [23]

3.2 Bone qualitative imaging

The USCT device, in this application, is a circular antenna having an internal radius of 150 mm and equipped with 8 fixed 1-MHz transducers distributed over a 360° angle ($\Delta\theta_{\text{fixed}} = 45^\circ$) [24]. The validity of USCT was tested on artificial and fresh bone sample. As fresh sample, in-vitro experiments were conducted on a fibula from a 10-year old child, containing water in the inner cavity. The mean cross-section of the bone was 17 ± 2 mm and that of the inner cavity

was 6 ± 2 mm. Figure 2 shows the USCT map (255×255 pixels) of the fibula. On the image, the outer and inner boundaries (i.e. the marrow area) were defined from image processing using an active contour method (Snake algorithm). If the outer contour is well defined, the resolution for the inner boundary is poor. The active contour method corrects its calculation by successive apodisations. This results in a smoothing of the boundary, which does not represent the actual bone area.

A human bone mimicking phantom (Sawbones™, tibia-fibula) was also studied. The cavity diameter of the tibia is 12.5mm. The fibula mimicking phantom had no inner cavity. The distance between bones was ~ 8 mm [24]. The USCT images of objects were compared with X-ray computed tomography (X-ray CT) images obtained at the same cross-section levels, with an X-ray CT device (Mediso™, Hungary) (Figure 2).

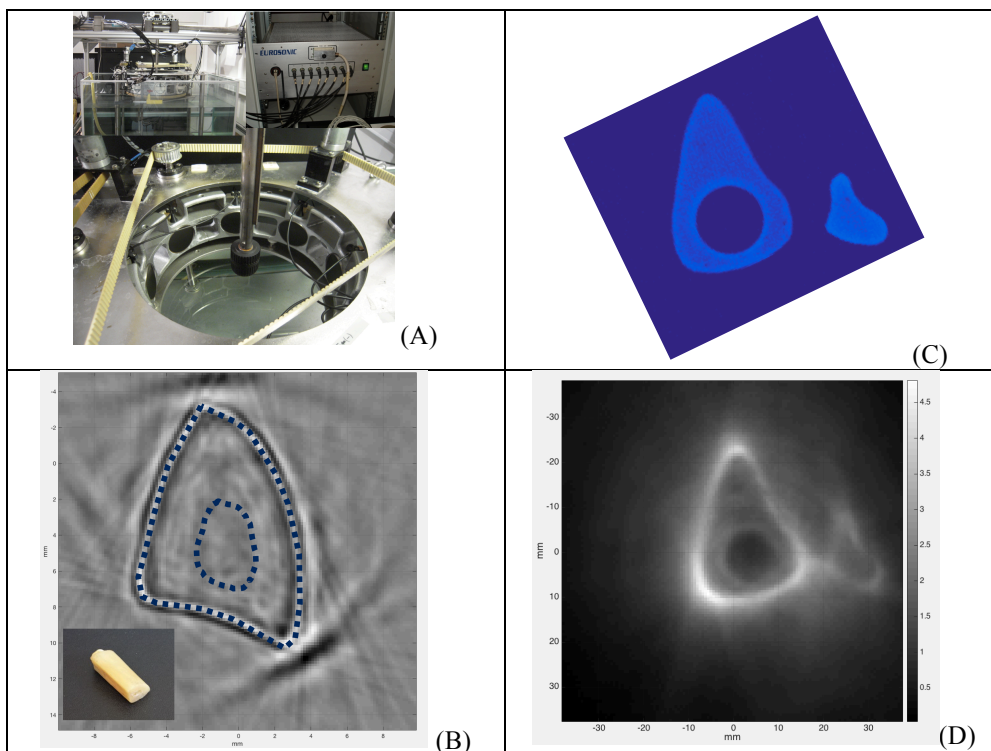
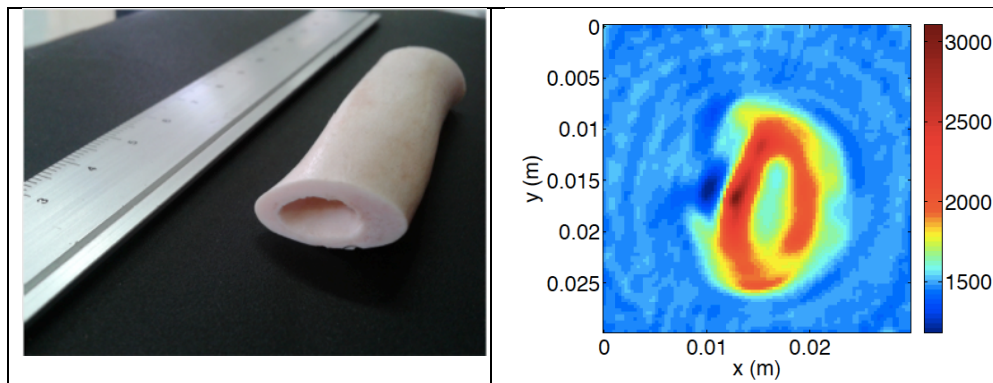


Figure 2: (A) Circular antenna with an internal radius of 150 mm, 8 fixed 1-MHz transducers (ImasonicTM), and a multiplexer electronic setup (8x8 channels, 12 bits, sampling frequency of 20 MHz) (Mistras-EurosonicTM) (B) The USCT-image of a child fibula. The inlaid picture shows the fresh bone sample. In dotted lines, the outer and inner boundaries are plotted using a Snake algorithm. (C) X-ray CT, and (D) USCT of a SawbonesTM composite bone-mimicking phantom. Details can be found in [24].

3.3 Bone quantitative imaging

The third results are obtained based on the non-linear schemes and quantitative USCT of bones. The first non-linear method (frequency-hopping method) was performed with a fresh and cleaned lamb shoulder bone, immersed in a water tank. Data acquisition was performed using a mechanical scanner, with one 500 kHz-transducer (ImasonicTM) as a transmitter, and one hydrophone (ResonTM) as a receiver. The usable bandwidth ranges from approximately 150 kHz to 750 kHz. The received signals were digitized (14 bits, 20 MHz) using a data acquisition sheet (Spectrum Mi4031). The sector scanned was 360 degrees with both transmitter and receiver, with an angular increment of 10 degrees (36 x 36 signals). The compressional wave and shear wave velocity in bone were respectively 2700 (\pm 200) m/s and 1250 (\pm 200) m/s (1476 m/s for the speed of sound in the water tank). Iterations were performed by gradually increasing the working frequency with four frequencies chosen within the useful bandwidth: 150 kHz, 250 kHz, 500 kHz and 750 kHz. Regarding the quantitative aspects, the compressional wave velocity was reconstructed with a relative error of about 30% [17].

For the full waveform inversion method, the results are purely numerical. No experimental results were obtained yet, but that will be the focus of future work. Figure 3 shows the main quantitative (compressional wave velocity and density) reconstruction obtained with a numerical phantom. The phantom has a realistic geometry of a tibia/fibula paired bone, surrounded by a water-like medium. The incident signal is a Ricker (second derivative of a Gaussian) 200 kHz-wavelet, and the virtual array has 8 sources and 128 receivers, with 9 cm of radius [21].



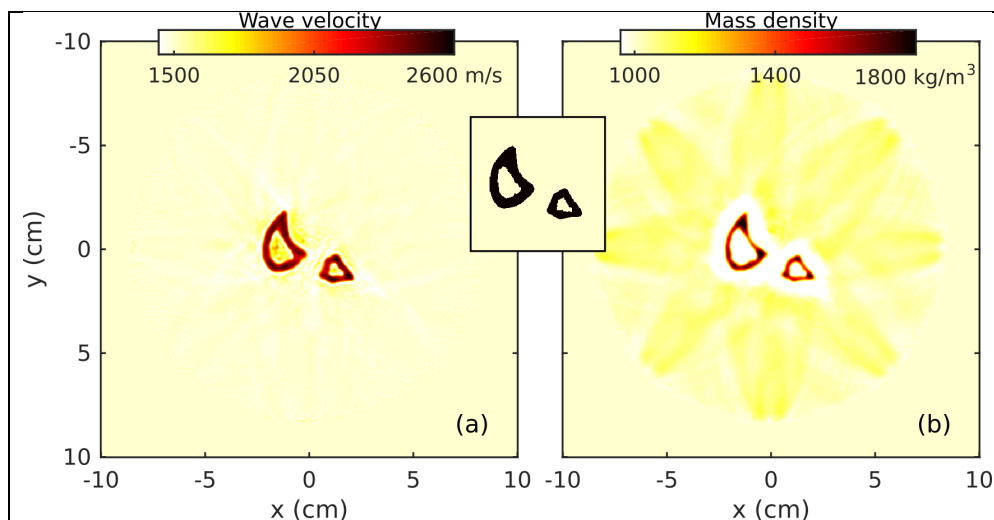


Figure 3: (Top) Experimental quantitative USCT of a lamb shoulder bone using non-linear frequency-hopping method. Images and details can be found in [17]. (Bottom) Numerical quantitative USCT of a tibia/fibula paired bone using non-linear full wave-form inversion method. Images and details can be found in [21].

4 Conclusions and future work

Ultrasonic Computed Tomography (USCT) appears as an alternative imaging tool capable of revealing the internal structure of soft tissues (mammography), delineating the shape of bones (cortical thickness), and even providing the possibility of parametric estimation (the sound speed and density map). In this work, the scope of USCT methods was extended from low impedance contrasted media such as soft tissues (the classical domain of USCT) to more contrasted domains such as cortical bone structures using non-linear and correction schemes. The wave field and associated Green function of the reference background medium were determined iteratively at the various steps. In future work, we plan to investigate various ways of improving these methods. Work is in progress, for instance, on the matrix inversion procedure involved in the FWI method and particularly on the regularization process, which is a very important aspect of the inversion scheme, especially in the case of high-contrast targets. Optimization, signal and image processing studies on how to handle the heavy experimental data are also ongoing (wavelet analysis, blind deconvolution, segmentation, Cramer-Rao bounds) [24]–[26].

Acknowledgements: The authors are grateful to Eric Debieu and Vincent Long at the Laboratory of Mechanics and Acoustics, (LMA) for their help in setting up experiments. The authors are grateful for medical assistance from Dr Philippe Petit and Dr Jean-Luc Jouve at the

"Timone" Children's Hospital (APHM). The X-ray CT were performed by Laure Balasse and Samantha Fernandez at the European Center for Research in Medical Imaging (CERIMED), Marseille.

References

- [1] S. Mensah and J.-P. Lefebvre, "Enhanced compressibility tomography," *IEEE Trans. Ultrason. Ferroelectr. Freq. Control*, vol. 44, no. 6, pp. 1245–1252, Nov. 1997.
- [2] S. Mensah and R. Ferriere, "Near-Field Diffraction Tomography," *Ultrason. Imaging*, vol. 24, no. 1, pp. 13–24, Jan. 2002.
- [3] S. Mensah and R. Ferriere, "Diffraction tomography: a geometrical distortion free procedure," *Ultrasonics*, vol. 42, no. 1–9, pp. 677–682, Apr. 2004.
- [4] P. Lasaygues, E. Ouedraogo, J.-P. Lefebvre, M. Gindre, M. Talmant, and P. Laugier, "Progress towards in vitro quantitative imaging of human femur using compound quantitative ultrasonic tomography," *Phys. Med. Biol.*, vol. 50, no. 11, pp. 2633–2649, Jun. 2005.
- [5] J. F. Greenleaf and R. C. Bahn, "Clinical Imaging with Transmissive Ultrasonic Computerized Tomography," *IEEE Trans. Biomed. Eng.*, vol. BME-28, no. 2, pp. 177–185, Feb. 1981.
- [6] M. P. André *et al.*, "A New Consideration of Diffraction Computed Tomography for Breast Imaging: Studies in Phantoms and Patients," in *Acoustical Imaging*, J. P. Jones, Ed. Boston, MA: Springer US, 1995, pp. 379–390.
- [7] N. V. Ruitter, T. O. Müller, R. Stotzka, and H. Gemmeke, "Evaluation of Different Approaches for Transmission Tomography in Ultrasound Computer Tomography," in *Bildverarbeitung für die Medizin 2005*, H.-P. Meinzer, H. Handels, A. Horsch, and T. Tolxdorff, Eds. Berlin/Heidelberg: Springer-Verlag, 2005, pp. 430–434.
- [8] N. Duric *et al.*, "Detection of breast cancer with ultrasound tomography: First results with the Computed Ultrasound Risk Evaluation (CURE) prototype: Detection of breast cancer with ultrasound tomography," *Med. Phys.*, vol. 34, no. 2, pp. 773–785, Jan. 2007.
- [9] E. Franceschini, S. Mensah, L. Le Marrec, and P. Lasaygues, "An optimization method for quantitative impedance tomography," *IEEE Trans. Ultrason. Ferroelectr. Freq. Control*, vol. 54, no. 8, pp. 1578–1588, Aug. 2007.
- [10] M. P. André, H. S. Janée, P. J. Martin, G. P. Otto, B. A. Spivey, and D. A. Palmer, "High-speed data acquisition in a diffraction tomography system employing large-scale toroidal arrays," *Int. J. Imaging Syst. Technol.*, vol. 8, no. 1, pp. 137–147, 1997.
- [11] R. C. Waag and R. J. Fedewa, "A ring transducer system for medical ultrasound research," *IEEE Trans. Ultrason. Ferroelectr. Freq. Control*, vol. 53, no. 10, pp. 1707–1718, Oct. 2006.
- [12] J. Rouyer, P. Lasaygues, and S. Mensah, "Novel Ultrasound Tomograph for Anatomical Inspection," in *Acoustical Imaging*, vol. 31, A. Nowicki, J. Litniewski, and T. Kujawska, Eds. Dordrecht: Springer Netherlands, 2012, pp. 3–10.
- [13] J.-P. Lefebvre, "Progress in linear inverse scattering imaging : NDE application of Ultrasonic Reflection Tomography," in *Inverse Problem in Engineering Mechanics*, Rotterdam/Brookfield: A.A.Balkema, 1994, pp. 371–375.

- [14] J. P. Lefebvre, P. Lasaygues, S. Mensah, S. Delamare, and A. Wirgin, "Born Ultrasonic Tomography: Some Limits and Improvements," in *Acoustical Imaging*, vol. 25, M. Halliwell and P. N. T. Wells, Eds. Boston: Kluwer Academic Publishers, 2002, pp. 79–86.
- [15] P. Lasaygues, R. Guillermin, and J.-P. Lefebvre, "Distorted Born diffraction tomography applied to inverting ultrasonic field scattered by noncircular infinite elastic tube," *Ultrason. Imaging*, vol. 28, no. 4, pp. 211–229, Oct. 2006.
- [16] R. Guillermin, P. Lasaygues, G. Rabau, and J.-P. Lefebvre, "Quantitative non-linear ultrasonic imaging of targets with significant acoustic impedance contrast—An experimental study," *J. Acoust. Soc. Am.*, vol. 134, no. 2, p. 1001, 2013.
- [17] R. Guillermin, P. Lasaygues, and G. Rabau, "Quantitative Ultrasonic Imaging of Bones," in *The 22nd International Congress on Sound and Vibration*, Florence, Italy, 2015, pp. 1–6.
- [18] J. Tromp, D. Komatitsch, and Q. Liu, "Spectral-Element and Adjoint Methods in Seismology," *Communications in Computational Physics*, pp. 1–32, 2008.
- [19] V. Monteiller, S. Chevrot, D. Komatitsch, and Y. Wang, "Three-dimensional full waveform inversion of short-period teleseismic wavefields based upon the SEM-DSM hybrid method," *Geophys. J. Int.*, vol. 202, no. 2, pp. 811–827, May 2015.
- [20] J. Nocedal and S. J. Wright, *Numerical optimization*. New York: Springer, 2006.
- [21] S. Bernard, V. Monteiller, D. Komatitsch, and P. Lasaygues, "Ultrasonic computed tomography based on full-waveform inversion for bone quantitative imaging," *Phys. Med. Biol.*, Jul. 2017.
- [22] J. Rouyer, S. Mensah, E. Franceschini, P. Lasaygues, and J.-P. Lefebvre, "Conformal ultrasound imaging system for anatomical breast inspection," *IEEE Trans. Ultrason. Ferroelectr. Freq. Control*, vol. 59, no. 7, pp. 1457–1469, Jul. 2012.
- [23] J. Rouyer, S. Mensah, C. Vasseur, and P. Lasaygues, "The benefits of compression methods in acoustic coherence tomography," *Ultrason. Imaging*, vol. 37, no. 3, pp. 205–223, Jul. 2015.
- [24] P. Lasaygues *et al.*, "Contrast resolution enhancement of Ultrasonic Computed Tomography using a wavelet-based method – Preliminary results in bone imaging," in *Proceedings of the Int. Workshop on Medical Ultrasound Tomography*, Speyer, Germany, 2017.
- [25] M. L. Diong, A. Roueff, P. Lasaygues, and A. Litman, "Precision analysis based on Cramer–Rao bound for 2D acoustics and electromagnetic inverse scattering," *Inverse Probl.*, vol. 31, no. 7, p. 075003, Jul. 2015.
- [26] M. L. Diong, A. Roueff, P. Lasaygues, and A. Litman, "Impact of the Born approximation on the estimation error in 2D inverse scattering," *Inverse Probl.*, vol. 32, no. 6, p. 065006, Jun. 2016.